# Accounts

## Surface Molecular Motion of Amorphous Polymeric Solids

**Tisato Kajiyama,* Keiji Tanaka, and Atsushi Takahara**

Department of Materials Physics and Chemistry, Graduate School of Engineering, Kyushu University, 6-10-1 Hakozaki, Higashi-ku, Fukuoka 812-81

(Received January 16, 1997)

Surface molecular motions of monodisperse polystyrene (PS) films, binary and ternary PS blend films, and polydisperse PS films were investigated on the basis of scanning force microscopic (SFM) measurements at 293 K. The monodisperse PSs were synthesized by a living anionic polymerization. It was revealed that the magnitude of the surface dynamic storage modulus $E'$ was remarkably lower than that for its bulk state, whereas, the surface dynamic loss tangent $\tan\delta$ value was fairly higher than that for its bulk state, in the case of the monodisperse PS with number-average molecular weight ($M_n$) lower than 26.6 k. The scanning viscoelasticity microscopic (SVM) measurements showed that the surface of the monodisperse PS film with $M_n$ lower than 26.6 k was in a glass–rubber transition state even at 293 K, even though the bulk $T_g$ was far above 293 K. Lateral force microscopic (LFM) measurements for the monodisperse PS films also revealed that the magnitude of lateral force was dependent on the scanning rate of the cantilever tip in the case of $M_n$ lower than 40.4 k. It is well accepted that the scanning rate dependence of lateral force appears in the case that the surface of the PS film is in a glass–rubber transition state. LFM results correspond well to SVM ones if the scanning rate of the cantilever tip for LFM measurement was converted to the measuring frequency for SVM measurement. Active thermal molecular motion on the polymeric solid surface was explained by the excess free volume induced due to the surface localization of chain end groups. The surface enrichment of chain end groups was confirmed by dynamic secondary ion mass spectroscopic (DSIMS) measurement.

The binary and the ternary PS blends were prepared by mixing the monodisperse PSs with different molecular weights. The commercially available PSs were also used as the polydisperse PS samples. LFM and SVM measurements revealed that the surface of the binary and the ternary PS blend films was in a glass–rubber transition state even at room temperature, when the component with $M_n$ lower than ca. 30 k existed. More active surface molecular motion compared with the bulk one for the binary and the ternary PS blend films can be explained by the surface segregation of the lower molecular weight component. The surface enrichment of lower molecular weight chains was confirmed on the basis of the DSIMS measurement by using the deuterated PS as the one component. In the case of the polydisperse PS film, even though the molecular weight distribution was broad and a somewhat lower molecular weight component was mixed, the active surface molecular motion showing a glass–rubber transition state was remarkably depressed at room temperature in comparison with the case for monodisperse PS film with the corresponding $M_n$s. The difference on the surface thermal molecular motion between monodisperse and polydisperse PS films might be explained on the basis of the chemical structure of the chain end groups. Also, in the case that the molecular weight component lower than ca. 30 k was not present in the system in spite of the broad molecular weight distribution, the surface molecular motion corresponding to the glass–rubber transition was not observed at room temperature.

Also, two-dimensional mapping of topography and surface $E'$ for the [PS/poly(methyl vinyl ether)] ultrathin blend film was carried out by using atomic force microscopy (AFM) and SVM, respectively. The combination of topographical and surface mechanical images could characterize the interfacial structure on nanometer scale.

Polymeric surfaces function as permselective membranes, biomaterials, adhesives, lubricants, and so on: these functions are closely related to surface aggregation structure and surface molecular motion.[1,2] Therefore, studies on surface aggregation structure and surface molecular motion for polymeric solids are quite important for practical applications as well as scientific interest. Surface aggregation structure has been investigated for several decades, both experimentally and theoretically, and many facts have been collected.[3—6] Only little information, however, has been reported on the surface molecular motion of the polymeric solids.

The authors proposed a new evaluation method for the surface glass transition temperature $T_g$ of the polymeric solids, based on the combination of temperature- and angular-dependent X-ray photoelectron spectroscopic (TDXPS and ADXPS) measurements and obtained the depth dependence

of the surface $T_g$ for the poly(styrene)-block-poly(methyl methacrylate) diblock copolymer [P(St-b-MMA)] films.[7,8] It was revealed that the surface $T_g$ was much lower than that for its bulk sample and also, the surface $T_g$ gradually increased along the direction away from the air/polymer interface.

Scanning force microscopy (SFM) is one of the new scanning probe microscopy techniques. It is important to investigate surface morphology of materials with high resolution.[9—11] The SFM image was created on the basis of the various forces acting between cantilever tip and sample surface, such as van der Waals, electrostatic, frictional, and magnetic force. When the SFM observation is carried out in a repulsive force region of the force curve, the sample surface might be deformed by the indentation of a tip. The modulation of the indentation leads to the modulation of the force acting between sample surface and cantilever tip. If the modulation of the tip indentation is applied sinusoidally to the sample surface, the dynamic viscoelastic properties at the sample surface can be evaluated by measuring the amplitude of the modulated deformation for the sample (response stress) and the phase lag between modulation signal (stimulation strain) and modulated deformation signal (response stress).[12—17]

The lateral force microscope (LFM) is also a useful tool for the two-dimensional mapping and/or the measurement of lateral force, which is evaluated by detecting the torsion of the sliding cantilever.[14,18] The lateral force measured by this technique is the sum of frictional and adhesion forces acting between sample surface and cantilever tip.[19] Since frictional force greatly depends on the surface relaxation behavior of polymeric materials,[20,21] it becomes possible to investigate the surface molecular motion on the basis of the scanning rate dependence of lateral force.[22]

The purpose of this study is to investigate the surface molecular motion of the amorphous polymeric solids by using scanning force microscopy.

**Setup of Scanning Viscoelasticity Microscope.** Figure 1 shows the block-diagram of the SVM apparatus.[15] The SFM equipment used in this study was SPA 300 (Seiko Instruments Industry Co., Ltd.) with an SPI 3700 controller. The specimen is mounted on an XYZ piezoscanner with a 20-μm scan range which has a resonance frequency of 15 kHz. The Z-sensitivity of the piezoelectric scanner is 4.46 nm $V^{-1}$. The cantilever tip is mounted on the piezoelectric bimorph actuator which has a resonance frequency of 1—10 kHz depending on the applied electric field. The bimorph consists of the alternating layers of metal electrodes, dielectric films, and piezoelectric zinc oxide films and can be bent vertically by applying opposite electric fields in the upper and lower piezoelectric sections.[23] The cantilever position in the Z-direction is modulated sinusoidally by applying an a.c. electric field, which is generated by the frequency generator (OSC), to the piezoelectric bimorph actuator. The deflection of the cantilever is measured by a position-sensitive four-segment photodiode (PSD) and feeds into the feedback loop that controls the height of the specimen. The modulated force is detected by the deflection of the cantilever. The deflection signal obtained with PSD is filtered by a band-pass filter (BPF) in order to reduce the high- and low-frequency noises and feeds a two-phase lock-in amplifier. The reference signal used is the sinusoidal signal from OSC, which corresponds to the dynamic strain signal.

**Surface Molecular Motion of Monodisperse PS Films.** The surface dynamic viscoelastic functions of the monodisperse PS films were evaluated on the basis of SVM measurements. The monodisperse PSs were prepared by a living anionic polymerization at 293 K using sec-butyllithium as an initiator. Table 1 shows number-average molecular weight, $M_n$ and the molecular weight dispersity, $M_w/M_n$, where $M_w$ is weight-average molecular weight. $M_n$ and $M_w/M_n$ were determined via gel permeation chromatography (GPC) with polystyrene standards. Bulk $T_g$ was evaluated on the basis of

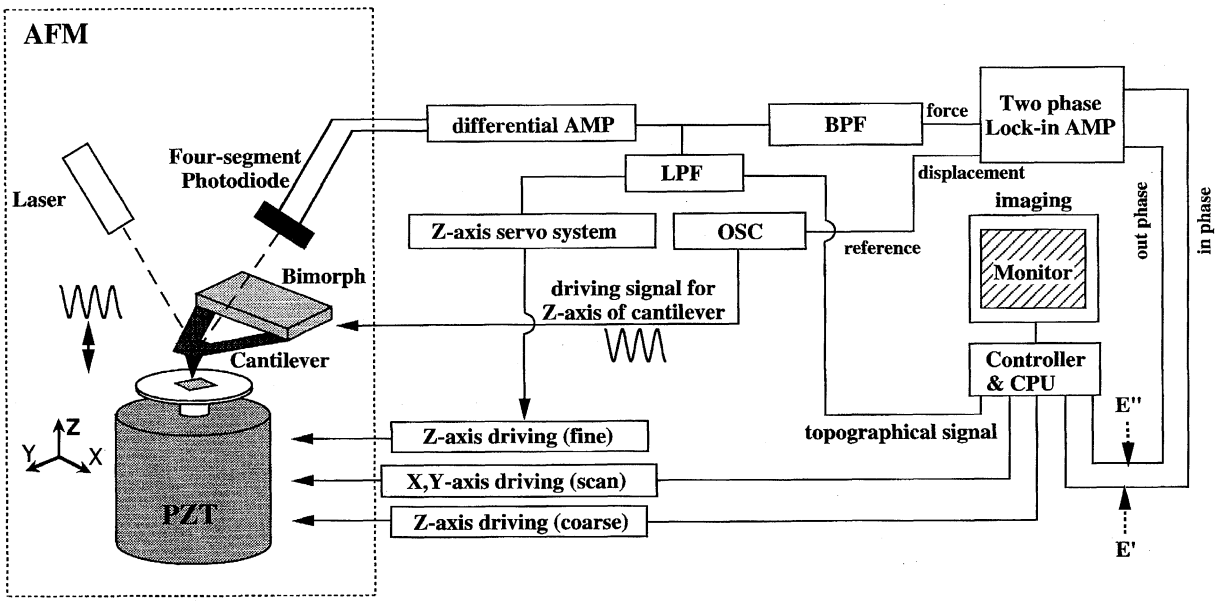


Fig. 1. Block-diagram of SVM equipment.

Table 1. Characterizations of Monodisperse PSs Used in This Study

| $M_n$ | $M_w/M_n$ |
|---|---|
| 1.7 k | 1.09 |
| 2.7 k | 1.10 |
| 4.9 k | 1.08 |
| 7.5 k | 1.09 |
| 9.0 k | 1.09 |
| 19.7 k | 1.07 |
| 26.6 k | 1.09 |
| 40.4 k | 1.08 |
| 47.5 k | 1.05 |
| 140.0 k | 1.06 |
| 218.6 k | 1.04 |
| 1800 k[a)] | <1.30 |

a) Purchased from Pressure Chemical Co., Ltd.

differential scanning calorimetric (DSC) measurements at a heating rate of 10 K $min^{-1}$ under dry nitrogen purge. The PS film of ca. 200 nm thick was coated from a toluene solution onto a cleaned silicon wafer by a spin-coating method at 2 krpm. The SVM measurement was performed at 293 K in air under a repulsive force of ca. 25 nN. The modulation frequency and the modulation amplitude were 4 kHz and 1.0 nm, respectively. A commercially available silicon nitride ($Si_3N_4$) cantilever with integrated tips (Olympus Co., Ltd.) was used. The spring constant of the cantilever was 0.09 N $m^{-1}$.

When a modulated deformation with an amplitude up to ca. 5 nm was applied to the monodisperse PS film, a linear relationship between amplitude of modulated deformation and out-put voltage as a stress signal was observed.[24] Since our SVM measurement was carried out under the static deformation of 1.1 nm and dynamic deformation of 1.0 nm, the linear surface dynamic viscoelastic characteristics were investigated for the monodisperse PS film. Static deformation, that is, the indentation depth of the tip, was evaluated on the basis of Hertz' elastic theory.[25] Figure 2 shows the schematic representation of the surface deformation by the indentation of the tip. The indentation depth $d$ of the tip was expressed as follows:

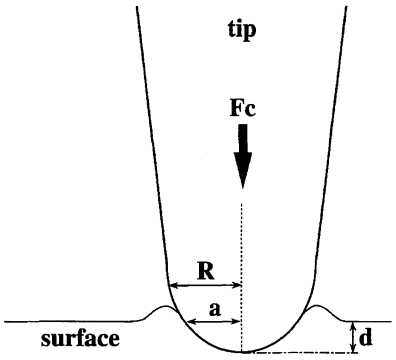


Fig. 2. The model describes the surface deformation by the indentation of the tip.

$$d = \left[\frac{9}{16}\left(\frac{1-\mu_{tip}^2}{E_{tip}} + \frac{1-\mu_{polymer}^2}{E_{polymer}}\right)^2 \frac{F_c^2}{R}\right]^{1/3}. \quad (1)$$

Here $\mu$, $E$, $R$, and $F_c$ are the Poisson ratio, modulus, the radius of curvature of the tip, and contact force, respectively. Since the tip is much harder than the sample, it is possible to neglect the first term in comparison with the second term in Eq. 1. The typical magnitudes of $E$ and $\mu$ for the glassy PS are 4.5 GPa and 0.33, respectively. Also, $R$ of 10 nm and $F_c$ of 25 nN were used for the evaluation of $d$.

Gaub et al. derived the surface dynamic storage modulus $E'$ and surface loss modulus $E''$ for the organic thin film in the case of forced oscillation SFM measurements with sample stage modulation.[13] Similarly, in the case of our SVM measurement with cantilever modulation, surface $E'$ and surface $E''$ of the polymeric film can be expressed as follows:

$$E' = (k_c \cdot H/\gamma)\cdot(\cos\phi - \gamma) \quad (2)$$

$$E'' = (k_c \cdot H/\gamma)\cdot\sin\phi, \quad (3)$$

where $k_c$, $\phi$, and $\gamma$ are a spring constant of the cantilever along the bent direction, an apparent phase lag between force and sample deformation, and a modulation ratio, respectively. Also, $H$ is a parameter related to the contact area between sample surface and probe tip and is called as a shape factor. From Eqs. 2 and 3, surface loss tangent, tan $\delta$ can be obtained by Eq. 4.

$$\tan\delta = E''/E' = \sin\phi/(\cos\phi - \gamma). \quad (4)$$

Since the magnitude of $k_c$ is known and the magnitudes of $\phi$ and $\gamma$ are obtained experimentally, the magnitudes of $E'$ and $E''$ can be determined after the magnitude of $H$ is evaluated. The electrical and mechanical phase lags of the instruments were calibrated by using a silicon wafer as a standard with a phase lag of zero.

The bulk dynamic viscoelastic properties for the PS film with $M_n$ of 1800 k were measured with a Rheovibron (DDV01-FP, Orientec Co., Ltd.). Figure 3 shows the temperature dependence of bulk $E'$ and bulk tan $\delta$ of the PS film with $M_n$ of 1800 k. The $\alpha_a$-dispersion behavior and the $\alpha_a$-absorption peak observed at ca. 390 K corresponds to the micro-Brownian motion of a main chain. The magnitudes of bulk $E'$ and bulk tan $\delta$ for the glassy PS film at 293 K were evaluated to be 4.5 GPa and 0.005, respectively.

The parts (a) and (b) of Fig. 4 show the molecular weight dependence of surface $E'$ and surface tan $\delta$ of the monodisperse PS films as well as the bulk tan $\delta$ and the bulk $T_g$ values evaluated by DSC. Before the magnitude of $H$ was determined, the $M_n$ dependence of the out-put voltage as a stress signal was obtained. Since, in a higher $M_n$ range from 40.4 k to 1800 k, the out-put voltage was almost constant, it can be considered that there is no $M_n$ dependence on the magnitude of $E'$, that is, the surface localization of chain ends is negligible. Especially, in the case of the PS film with $M_n$ of 1800 k, since the concentration of chain end groups

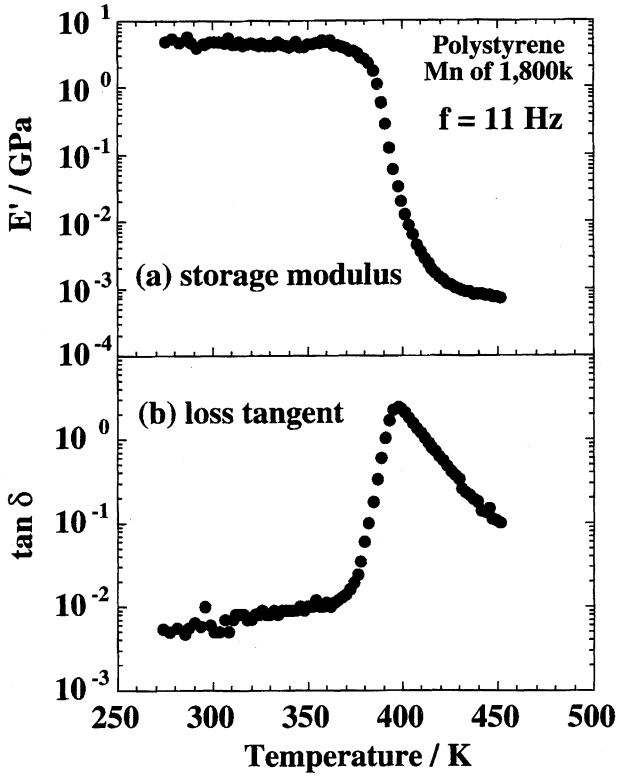


Fig. 3. Temperature dependence of (a) bulk dynamic storage modulus $E'$ and (b) bulk loss tangent tan $\delta$ for the PS film with $M_n$ of 1800 k as a standard. The measurement was performed at a frequency of 11 Hz by using a Rheovibron.

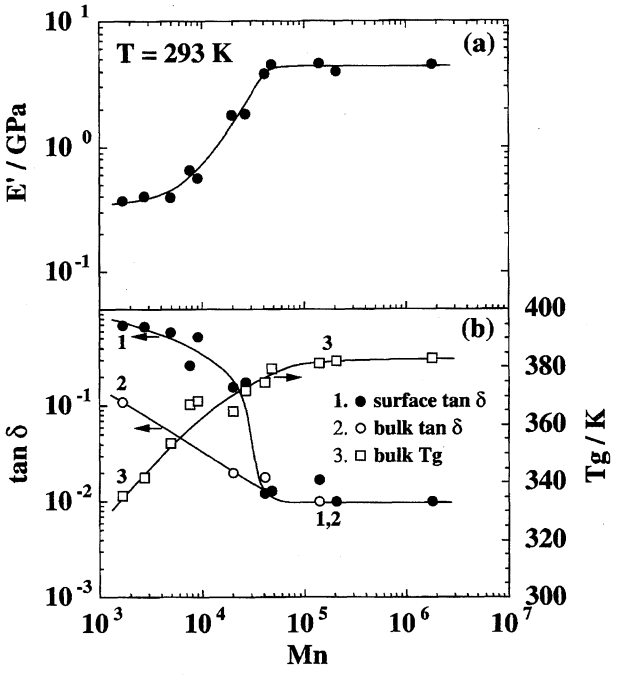


Fig. 4. Molecular weight dependence of (a) surface dynamic storage modulus, $E'$ and (b) surface loss tangent, tan $\delta$ for the monodisperse PS film. The open circles in (b) show bulk tan $\delta$.

is extremely low, it seems reasonable to assume that thermal molecular motion at the film surface is comparable to that for the bulk sample even if chain end groups are preferentially segregated at the film surface. Then, on the assumption that the surface $E'$ is same as the bulk $E'$ at 293 K, the magnitude of $H$ can be decided. Since the magnitudes of apparent phase lag between force and sample deformation $\phi$ and the ratio of modulation amplitudes $\gamma$ were experimentally measured, the magnitudes of surface $E'$ and surface tan $\delta$ for the PS films with various $M_n$ were evaluated by using Eqs. 2 and 4. In a $M_n$ range larger than 40.4 k, the magnitudes of surface $E'$ and surface tan $\delta$ were constant; their magnitudes were ca. 4.5 GPa and 0.01, respectively. Then, it seems reasonable to conclude from the magnitudes of surface $E'$ and surface tan $\delta$ that the surface of the PS film with larger $M_n$ than 40.4 k is in a glassy state at 293 K. Also, in the case of $M_n$ smaller then 26.6 k, as shown in Fig. 4, the magnitudes of surface $E'$ and surface tan $\delta$ decreased and increased with a decrease in $M_n$, respectively. The magnitudes of surface $E'$ and surface tan $\delta$ indicate that the surface of the PS film with smaller $M_n$ than ca. 30 k is in a glass–rubber transition state even at 293 K. Dynamic viscoelastic properties of the monodisperse bulk PS sample were measured in order to compare the bulk $E'$ with the surface $E'$. Since, in the case of $M_n$ smaller than 40.4 k, the film was very fragile, dynamic spring analysis technique was applied to evaluate bulk tan $\delta$.[26] In the case of $M_n$ smaller than ca. 30 k, the magnitude of surface tan $\delta$ was much higher than that of bulk tan $\delta$ as shown in Fig. 4(b). This clearly indicates that the surface $T_g$ of the PS film is more strongly dependent on $M_n$ than the bulk $T_g$, because the preferential surface localization of chain end groups becomes more prominent in the case of the smaller $M_n$. Thus, it seems reasonable to conclude that thermal molecular motion at the film surface is more active in comparison with that for the bulk sample, especially in the case of $M_n$ smaller than ca. 30 k.

In order to investigate the relaxation behavior of the PS film surface, an LFM measurement was carried out at 293 K in air under a repulsive force of ca. 25 nN. LFM equipment used in this study was SPA 300 (Seiko Instruments Industry Co., Ltd.) with an SPI 3700 controller. The cantilever used in LFM measurement was the same as SVM measurement.

Figure 5 shows the schematic representation of frequency dependence of dynamic loss modulus $E''$ for the polymeric solids.[27] In the case of very high or low frequency ranges, the polymer film is in a glassy state or a rubbery one, respectively, and has a low magnitude of $E''$. On the other hand, in an intermediate frequency region, the polymer film is in a glass–rubber transition state and then exhibits the peak of $E''$. Hereupon, we consider the scanning rate dependence of lateral force that directly corresponds to the frequency dependence of the surface mechanical property. The frequency $f$ is proportional to an inverse of a period $T$

$$f = 1/T, \tag{5}$$

and also, $T$ can be expressed as,

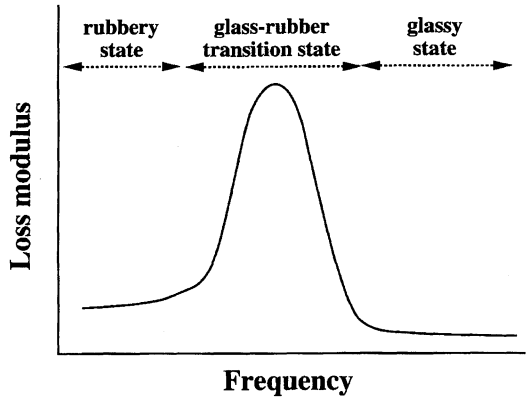


Fig. 5. Schematic representation of the frequency dependence of loss modulus, $E''$.

$$T = 2a/v, \tag{6}$$

where $a$ and $v$ are the contact radius as shown in Fig. 2 and the scanning rate of the tip, respectively. According to Hertz' elastic theory, $a$ can be expressed as follows:

$$a = \left[\frac{3}{4}\left(\frac{1-\mu_{\text{tip}}^2}{E_{\text{tip}}} + \frac{1-\mu_{\text{polymer}}^2}{E_{\text{polymer}}}\right) RF_c\right]^{1/3}. \tag{7}$$

As Eqs. 5 and 6 are substituted into Eq. 7, the relationship between frequency and scanning rate can be expresses as follows:

$$f = \frac{v}{2}\left[\frac{3}{4}\left(\frac{1-\mu_{\text{tip}}^2}{E_{\text{tip}}} + \frac{1-\mu_{\text{polymer}}^2}{E_{\text{polymer}}}\right) RF_c\right]^{-1/3}. \tag{8}$$

Then, the abscissa $f$ of Fig. 5 can be replaced by the scanning rate $v$.

Next, the relationship between $E''$ and lateral force will be discussed. Figure 6 shows the schematic illustration of the surface deformed by a sliding tip. When the tip slides on the polymer surface, a rim is produced ahead of the tip, as shown in the upper part of Fig. 6. In the case of the glassy surface, elastic energy is stored in the front rim. However, since the relaxation time is very short, the deformed surface behind the sliding tip is quickly recovered and then, elastic energy is imparted to the sliding tip. As a consequence, the total energy loss is small, that is, the frictional force is small. When the surface is in a rubbery state, the amount of energy to produce the front rim is small due to the small magnitude of its $E'$. Even though the determined surface behind a sliding tip can not be relaxed quickly because of its long relaxation time, the frictional force becomes small because of the small magnitude of $E'$. On the other hand, in the case that the surface is in a glass–rubber transition state, the energy required for the formation of the front rim is larger than that for the glassy or rubbery state, due to its fairly large $E''$. Moreover, the deformed surface does not relax quickly. Therefore, the magnitude of frictional force becomes larger. Since the magnitude of frictional force is almost proportional to the loss modulus, as mentioned previously in Fig. 5, the $E''$ ordinate in Fig. 5 can be replaced by the frictional force, as shown in the lower part of Fig. 6.

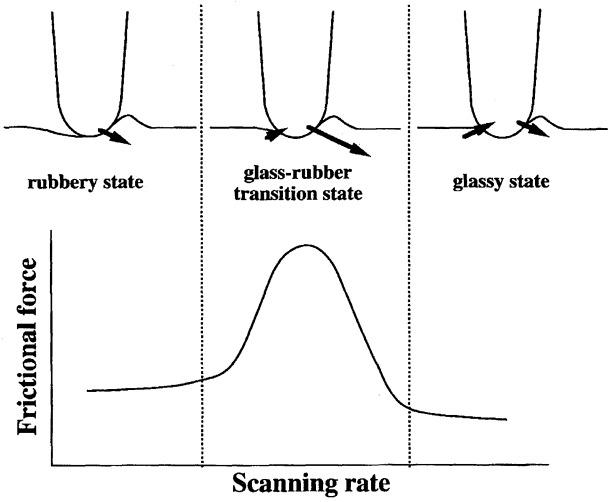


Fig. 6. Schematic illustration of the deformed surface by a sliding tip. The length of an arrow shows the magnitude of energy imparted.

Figure 7 shows the plots of lateral force against the scanning rate as a function of $M_n$. The tip indent depth of ca. 1.1

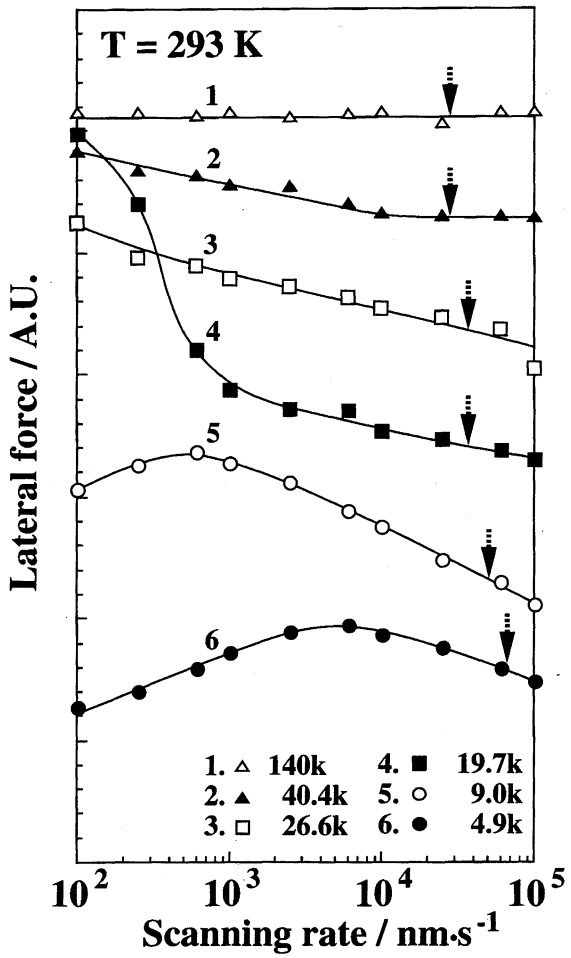


Fig. 7. Scanning rate dependence of lateral force of the PS film as a function of the number-average molecular weight. Each curve is shifted arbitrarily along the ordinate. The broken arrow shows the scanning rate corresponding to the frequency of the SVM measurement.

nm was comparable to the magnitude of static deformation for SVM measurement. The broken arrows in the Figure denote the scanning rates corresponding to the frequency of SVM measurements, which were calculated by Eq. 8. The lateral force measured by LFM is the sum of frictional force and adhesion force.[19] Since the scanning rate dependence of adhesion force is negligible,[28] the scanning rate dependence of lateral force indicates that frictional force strongly depends on the scanning rate. Since no distinct scanning rate dependent of lateral force was observed in the case of $M_n$ of 140.0 k, it seems reasonable to conclude that the surface is in a glassy state. On the other hand, the lateral force the PS film surface with $M_n$ less than 40.4 k was apparently dependent on the scanning rate. In the case of $M_n$ of 40.4 k, although no scanning rate dependence of lateral force was observed at a high scanning rate region, the magnitude of lateral force was affected by the scanning rate in the low scanning rate region. Then, LFM measurements for the PS film with $M_n$ of 40.4 k at low and high scanning rates exhibit clearly the existence of a glass–rubber transition state and a glassy one, respectively. Since SVM measurement for the PS film with $M_n$ of 40.4 k was performed at 4 kHz corresponding to a high scanning rate of $2.7\times10^4$ nm s$^{-1}$, the surface $E'$ of 4.5 GPa was quite reasonable. In the cases of $M_n$ of 26.6 k and 19.7 k, since the lateral force decreased with an increase in scanning rate, it can be concluded that the surface is in a glass-transition state at 293 K. Moreover, in the case of $M_n$ of 9.0 k and 4.9 k, the peak of lateral force was clearly observed on the lateral force-scanning rate curve. These results indicate that surface $E''$ has the maximum value in the scanning rate region employed in this study, that is, the surface of the PS film with $M_n$ of 9.0 k and 4.9 k is in a glass–rubber transition state at 293 K. Since the surface $T_g$ for the PS film with $M_n$ of 9.0 k is higher than that for $M_n$ of 4.9 k, it is reasonable that the peak on the lateral force-scanning rate curve for the PS film with $M_n$ of 9.0 k appears in a lower scanning rate region in comparison with that for $M_n$ of 4.9 k.

A depression $T_g$ at the film surface compared with that for the bulk sample has been explained by the surface localization of chain end groups.[8] However, the relationship between surface localization of chain end groups and surface molecular motion has not been experimentally confirmed. Deuterated polystyrene (dPS) in which the chain end groups were labelled by protonated groups was prepared. Dynamic secondary ion mass spectroscopic (DSIMS) measurements were performed in order to confirm the surface localization of chain end groups. Figure 8 shows the chemical structure of end-labelled dPS used in this study. End-labelled dPS was prepared by a living anionic polymerization. Only each end portion was labelled with a proton. DSIMS analysis was performed using SIMS 4000 (Seiko Instruments Inc. -Atomika Analysetechnik GmbH). The incident beam of oxygen ions with 3.0 keV and 6—7 nA was focused onto a 100 μm×100 μm area of the specimen surface. A platinum layer of 10 nm thick was sputter-coated on the surface of the end-labelled dPS film in order to avoid charging up of the specimen during the DSIMS measurement.

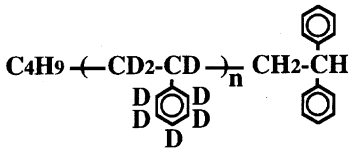


Fig. 8. Chemical structure of end-labelled dPS.

Figure 9 shows the typical SIMS depth profile of the end-labelled dPS film. The dashed vertical line corresponds to the air/polymer interface. The intensity of carbon ion $C^+$ was almost constant at any depth position from the polymer film surface and the steady-state etching proceeded during the etching process. Although, in general, the secondary ion efficiency of a hydrogen atom is higher than that of a heavy hydrogen atom, the stronger intensity of deuterium ion $D^+$ than that of proton $H^+$ was maintained during the etching of the polymer film. This stronger intensity of $D^+$ results from the larger fraction of heavy hydrogen atom in the end-labelled dPS. Figure 9 revealed an apparent increase in the intensity of $H^+$ and a decrease in that of $D^+$ in the air/polymer interface region. Since the styrene unit was deuterated, protons were present only in both chain end portions. Thus, the SIMS depth profile apparently shows a remarkable enrichment of chain end groups at the air/polymer interface. Since the surface localization of chain end groups induces some excess free volume fraction at the film surface compared with that in the bulk phase, it seems reasonable to conclude that the surface $T_g$ is lower than the bulk $T_g$. The result is that surface molecular motion at the film surface is more active in comparison with that for the bulk sample at room temperature.

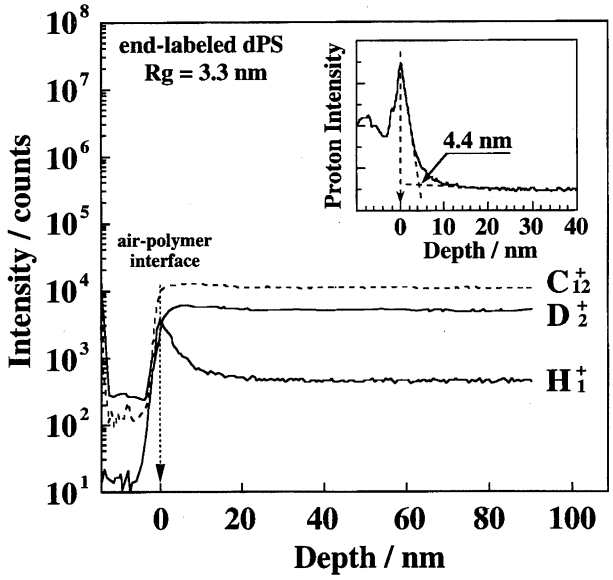


Fig. 9. SIMS depth profile of proton, deuterium and carbon ions for the end-labelled deuterated PS film. The inset enlarges the proton intensity profile in linear scale at the vicinity of the air–polymer interface. The depth before the attainment of the dashed vertical line corresponds to sputtering the platinum layer of 10 nm thick to avoid charging of the specimen during SIMS measurement.

As shown in Fig. 10, the localization decay length of chain end groups was defined as the range from the air/polymer interface to the depth that the initial slope of $H^+$ profile crossed the bulk intensity. The localization decay length of chain end groups was 4.4 nm and its value was almost comparable to the radius of gyration of an unperturbed chain, $R_g$ of 3.3 nm.

**Surface Molecular Motion of Polydisperse PS Films.** In this section, surface molecular motions for the binary and the ternary PS blend films composed of monodisperse PSs as a model for the polydisperse PS and also the commercially available polydisperse PS films, which are industrially important, will be discussed. Table 2 shows the physicochemical properties such as $M_n$, $M_w/M_n$, and the bulk $T_g$ for the PS blends and the polydisperse PSs used in this study. The binary and the ternary PS blends were prepared by mixing monodisperse PSs, which were synthesize by living anionic polymerization. The polydisperse PSs were commercially available. The PS films of ca. 200 nm thick were coated from a toluene solution onto a silicon wafer with native oxide layer by a spin-coating method. SVM and LFM measurements of the PS blend and the polydisperse PS films were carried out under the same conditions as those for monodisperse PS systems mentioned previously.

Surface molecular motion, that is, the scanning rate dependence of lateral force for the binary and the ternary PS blends, has been investigated. Figure 11 shows the scanning rate dependence of lateral force for the Binary 1 film at 293 K. The Binary 1 was prepared by mixing monodisperse PSs with $M_n$ of 19.7 k and deuterated PS (dPS) with $M_n$ of 1000 k. The blend ratio of (PS/dPS) was (5/95) in weight. The filled and the open circles correspond to the lateral force for the as-cast Binary 1 film and the annealed one at 393 K for

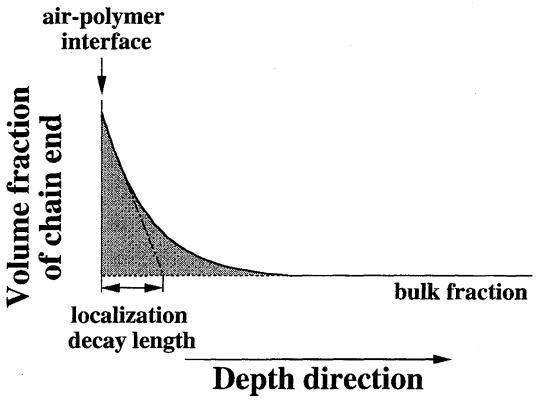


Fig. 10. Definition of localization decay length.

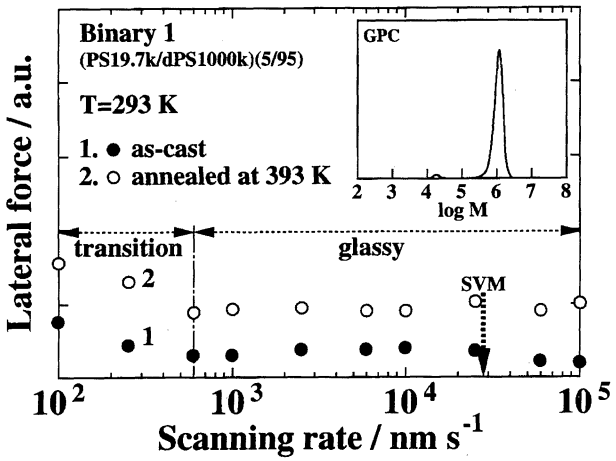


Fig. 11. Scanning rate dependence of lateral force for the Binary 1 film at 293 K. The filled and the open circles denote the lateral force for the as-cast Binary 1 film and annealed one at 393 K for 24 h, respectively. The inset in Fig. 11 shows the molecular weight distribution of Binary 1 system evaluated by GPC measurement. The broken arrow in Fig. 11 shows the scanning rate corresponding to the frequency of SVM measurement.

24 h, respectively. The inset in Fig. 11 shows the molecular weight distribution of the Binary 1 system, evaluated by GPC measurement. Also, the broken arrow shows the scanning rate corresponding to the frequency of SVM measurement. Both films did not exhibit the distinct scanning rate dependence of lateral force at a higher scanning rate range $6\times10^2$ nm $s^{-1}$. Yet, the magnitude of lateral force increased with a decrease in the scanning rate at scanning rate region lower than $6\times10^2$ nm $s^{-1}$. Then, Fig. 11 indicates that the surface is in a glass–rubber transition state and in a glassy one at lower and higher scanning rate regions, respectively, even at 293 K. The magnitude of surface $E'$ and surface tan $\delta$ for the as-cast Binary 1 film evaluated by SVM measurement at 293 K were 4.3 GPa and 0.02. This clearly shows that the surface is in a glassy state at the scanning rate corresponding to SVM measurement. Based on the result of Fig. 7, it is reasonable to consider that the scanning rate dependence of lateral force for the Binary 1 film might arise from the component of monodisperse PS with $M_n$ of 19.7 k.

In order to confirm the surface molecular motion-structure relationship for the Binary 1 film mentioned above, DSIMS measurement was carried out. Figure 12 shows the SIMS depth profile of proton $H^+$ and deuterium ion $D^+$ for the Binary 1 film annealed at 393 K for 24 h. The dashed vertical lines of left and right hand sides correspond to the air/polymer

Table 2. Characterizations of PS Blends and Polydisperse PSs Used in This Study

| Sample | $M_n$ | $M_w/M_n$ | $T_g$/K | Remarks |
|---|---|---|---|---|
| Binary 1 | 370 k | 3.49 | 377.9 | (PS19.7 k/dPS1000 k) (5/95/ w/w) |
| Binary 2 | 36 k | 2.52 | 376.8 | (PS19.7 k/PS140 k) (50/50 w/w) |
| Ternary | 65 k | 7.17 | 379.6 | (PS19.7 k/PS219 k/PS1460 k) (25/50/25 w/w/w) |
| Polydisperse 1 | 29 k | 6.26 | 375.5 | HF11 |
| Polydisperse 2 | 169 k | 2.67 | 377.8 | US305 |

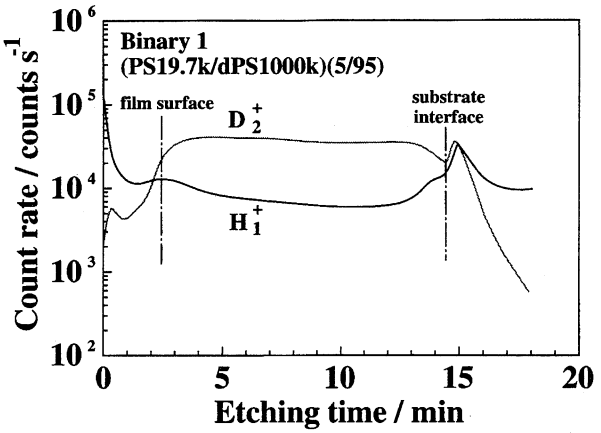


Fig. 12. SIMS depth profile of proton and deuterium ion for the Binary 1 film. The dashed vertical lines of left and right hand sides correspond to the air/polymer and the polymer/substrate interfaces, respectively.

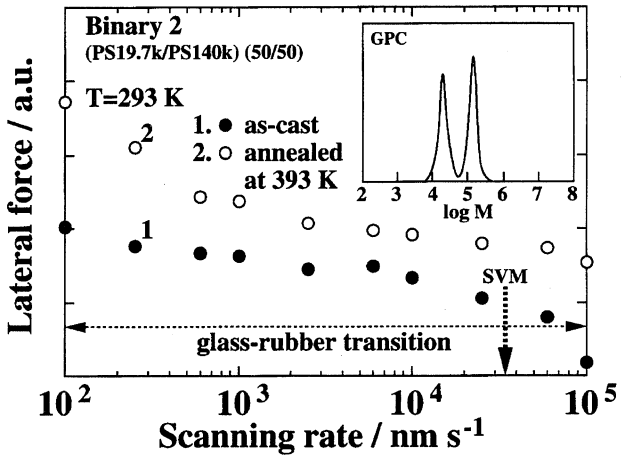


Fig. 13. Scanning rate dependence of lateral force for the Binary 2 film at 293 K. The filled and the open circles denote the lateral force for the as-cast Binary 2 film and annealed one at 393 K for 24 h, respectively. The inset in this Figure shows the molecular weight distribution of Binary 2 system. The broken arrow in the Fig. 13 shows the scanning rate corresponding to the frequency of SVM measurement.

interface and the polymer/substrate one, respectively. The initial etching region prior to the air/polymer interface corresponds to the platinum layer which was used to avoid charge-up of the polymer film during measurement. The proton and deuterium ion intensities apparently increased and decreased at the air/polymer interface and the polymer/substrate one, respectively. Since only the lower molecular weight component, that is PS with $M_n$ of 19.7 k, was protonated, Fig. 12 apparently shows that the lower molecular weight component was preferentially segregated at both interfaces. It should be noted that the lower molecular weight component was enriched at the film surface in spite of the higher surface free energy component due to the higher polarizability of C–H bond compared with that of C–D bond. With respect to the surface segregation of the lower molecular weight component, we should consider mainly two factors: The enthalpy term, that is, the magnitude of surface free energy of chain end groups; and the entropy term, the conformational entropy loss of the chain present at the film surface. A more detailed explanation on the surface enrichment of the lower molecular weight component will be discussed elsewhere.[29] Since the concentration of the chain end groups is proportional to $2/N$, where $N$ is the degree of polymerization, the surface segregation of the lower molecular weight component induces an excess free volume at the film surface, resulting in more activated surface molecular motion in comparison with the higher molecular component. Thus, it seems reasonable to conclude that the surface of the Binary 1 film is in a glass–rubber transition state even at 293 K, due to the surface localization of the lower molecular weight component at the lower scanning rate range, though the bulk $T_g$ is 378 K.

Figure 13 shows the scanning rate dependence of lateral force for the Binary 2 film at 293 K. The Binary 2 was prepared by mixing monodisperse PSs with $M_n$s of 19.7 k and 140.0 k with the blend ratio of (50/50) in weight. The filled and the open circles show the lateral force for the as-cast Binary 2 film and the annealed one at 393 K for 24 h, respectively. The inset in Fig. 13 shows the molecular weight distribution of the Binary 2 system evaluated by GPC measurement. The lateral force of the as-cast Binary 2 film increased with a decrease in the scanning rate in all scanning rate regions studied here. The magnitudes of surface $E'$ and surface tan $\delta$ evaluated by SVM measurement at 293 K were 2.3 GPa and 0.05, respectively. These LFM and SVM results indicate that the surface of the as-cast Binary 2 film is in a glass–rubber transition state even at 293 K. Since the magnitudes of surface $E'$ and surface tan $\delta$ for the monodisperse PS film with $M_n$ of 19.7 k were 1.8 GPa and 0.15, respectively, as shown in Fig. 4, it appears that the PS with $M_n$ of 19.7 k is preferentially segregated at the film surface. When the Binary 2 film was annealed at 393 K for 24 h, the scanning rate dependence of the lateral force become more pronounce than that for the as-cast one. Its scanning rate-lateral force curve is similar to that for the monodisperse PS film with $M_n$ of 19.7 k as shown in Fig. 7. Then, it seems reasonable to conclude that the PS with $M_n$ of 19.7 k is more enriched at the film surface by annealing the Binary 2 film at 393 K for 24 h, and then the surface molecular motion becomes more activated than that of the as-cast Binary 2 film.

The investigation of surface molecular motion has been extended to the Ternary PS blend system. Figure 14 shows the scanning rate dependence of lateral force for the Ternary film at 293 K. The ternary PS blend system was composed of monodisperse PSs with $M_n$s of 19.7 k, 219 k, and 1460 k with blend ratio of (25/50/25) in weight. The filled and the open circles show the lateral force for the as-cast Ternary film and the annealed one at 393 K for 24 h, respectively. Since the as-cast Ternary film and the annealed one showed distinct scanning rate dependences of lateral force, it seems reasonable to conclude that surface molecular motion is activated in

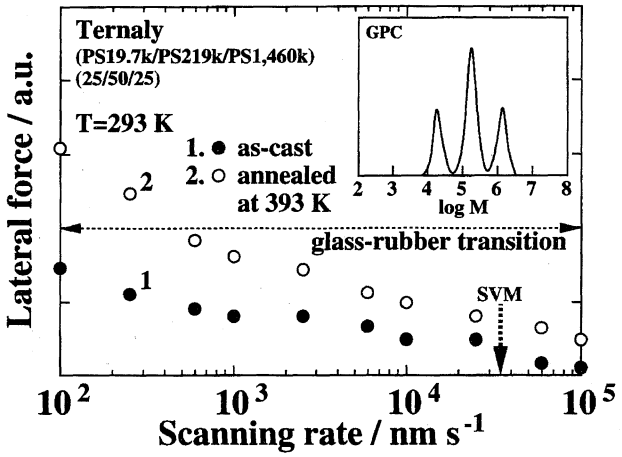


Fig. 14. Scanning rate dependence of lateral force for the Ternary film at 293 K. The filled and the open circles denote the lateral force for the as-cast Ternary film and annealed one at 393 K for 24 h, respectively. The inset in this Fig. 14 shows the molecular weight distribution of Ternary PS blend. The broken arrow in the Fig. 14 shows the scanning rate corresponding to the frequency of SVM measurement.

comparison with the bulk one due to the preferential surface segregation of PS with $M_n$ of 19.7 k. Since annealing of the film induces more effective surface localization of PS with smaller $M_n$, the scanning rate dependence of lateral force for the annealed one become more pronounced in a similar fashion to the Binary blend film. The magnitudes of surface $E'$ and surface tan $\delta$ for the Ternary film at 293 K were 2.3 GPa and 0.07, respectively. Therefore, the SVM measurement also exhibited the surface in a glass–rubber transition state.

Figure 15 shows the scanning rate dependence of lateral force for the commercially available Polydisperse 1 film at

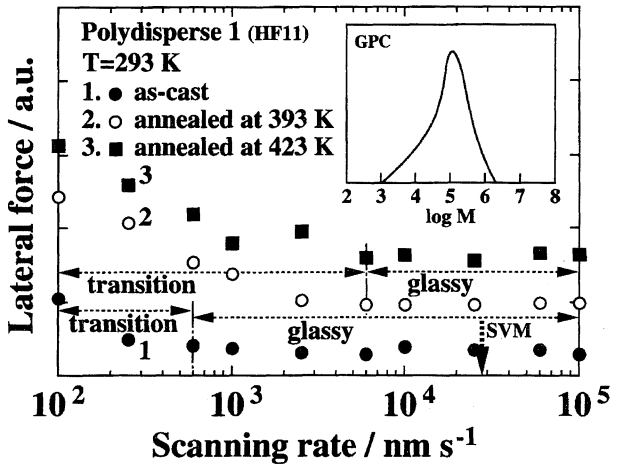


Fig. 15. Scanning rate dependence of lateral force for the Polydisperse 1 film at 293 K. The filled circles, the open circles and the filled squares denote the lateral force for the as-cast Polydisperse 1 film, films annealed at 393 K and at 423 K for 24 h, respectively. The inset in this Figure shows the molecular weight distribution of Polydisperse 1 system. The broken arrow in the Fig. 15 shows the scanning rate corresponding to the frequency of SVM measurement.

293 K. The filled circles, the open ones, and the filled squares show the results for the as-cast Polydisperse 1 film, the film annealed at 393 K for 24 h and those annealed at 423 K for 24 h, respectively. In the case of the as-cast Polydisperse 1 film, the scanning rate dependence of lateral force was not apparent at scanning rates higher than $6\times10^2$ nm s$^{-1}$ and the lateral force slightly increased with a decrease in the scanning rate at the scanning rates lower than $6\times10^2$ nm s$^{-1}$. This indicates that, at the lower scanning rate region, the surface is in an initial stage of a glass–rubbery transition even at 293 K. The magnitudes of surface $E'$ and surface tan $\delta$ for the as-cast Polydisperse 1 film evaluated by SVM measurement at 293 K were 4.4 GPa and 0.02, respectively, indicating a glassy state at a corresponding scanning rate shown by the broken arrow in Fig. 15. When the annealing treatment for the Polydisperse 1 film was carried out at 393 K or 423 K for 24 h, the scanning rate dependence of lateral force became more distinct up to $2.5\times10^3$ nm s$^{-1}$. However, the scanning rate-lateral force curves are very similar between the two annealed films. These results indicate that, when the annealing treatment of the Polydisperse 1 film was performed, the lower molecular weight component was preferentially segregated at the film surface and the annealing effect was almost the same in the case of annealing above bulk $T_g$. The Polydisperse 1 system has broad molecular weight distribution and contains much lower molecular weight components, as shown by the inset in Fig. 15. Even though a fairly high fraction of the lower molecular weight component with $M_n$ values lower than ca. 30 k was contained in the Polydisperse 1 system, the scanning rate dependence of lateral force corresponding to a glass–rubber transition state was not distinct in comparison with that for the monodisperse PS film with $M_n$ smaller than ca. 30 k as shown in Fig. 7. This difference might be explained on the basis of the chemical structure of chain end groups, as shown in Fig. 16. Figure 16 shows the schematic representation of the molecular aggregation state of a polymeric chain at the air/polymer interface for PSs prepared by living anionic and radical polymerizations. When chain end groups have lower surface free energies compared with the main chain part, the chain end group is preferentially localized at the film surface.[30] In the case of the PS prepared by living anionic polymerization using *s*-butylithium as an initiator, one of chain end groups and the another one are

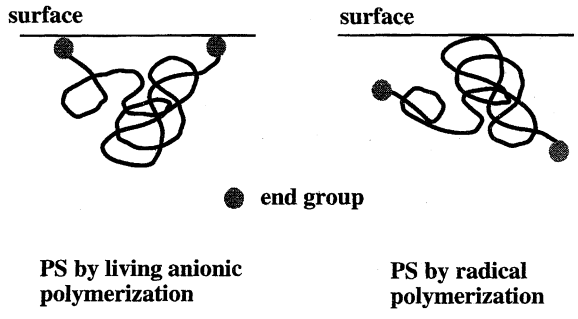


Fig. 16. Schematic illustration of the molecular aggregation state for PSs prepared by living anionic and radical polymerizations at the film surface.

composed of butyl group and repeating unit, respectively. In this case, since the magnitudes of the surface free energy for the chain end groups are smaller than that of the main chain,[31] chain end groups are preferentially segregated at the film surface, as shown in Fig. 9. In the cases of the PS prepared by radical polymerization using $\alpha,\alpha'$-azobisisobutyronitrile, redox initiator and so on, however, the hydrophilic fragments are incorporated into the chain ends because the polymerization reaction is terminated completely by recombination. Then, since chain end groups have higher surface free energy in comparison with the main chain, chain end groups might migrate into the surface region part from the air/polymer interface. Even if the lower molecular weight component is preferentially segregated at the film surface in the case of the PS prepared by radical polymerization, the end group concentration at the film surface is not increase effectively. Therefore, it seems reasonable to conclude that, in the case of the polydisperse PS film prepared by radical polymerization, the remarkable activation of the surface molecular motion induced by the surface segregation of chain end groups as measured for the monodisperse PS film with smaller $M_n$, is not apparently detected due to the preferential migration of chain end groups into a deeper surface region from the air/polymer interface.

Figure 17 shows the scanning rate dependence of lateral force for the Polydisperse 2 film at 293 K. The filled and the open circles show the lateral force for the as-cast Polydisperse 2 film and the annealed one at 393 K for 24 h, respectively. In both cases, no distinct scanning rate dependence of lateral force was observed, because the fraction of the lower molecular weight component with $M_n$ smaller than 30 k is very low. Also, the magnitudes of surface $E'$ and surface tan $\delta$ for the as-cast Polydisperse 2 film based on SVM measurement at 293 K were 4.3 GPa and 0.02, respectively. The LFM and

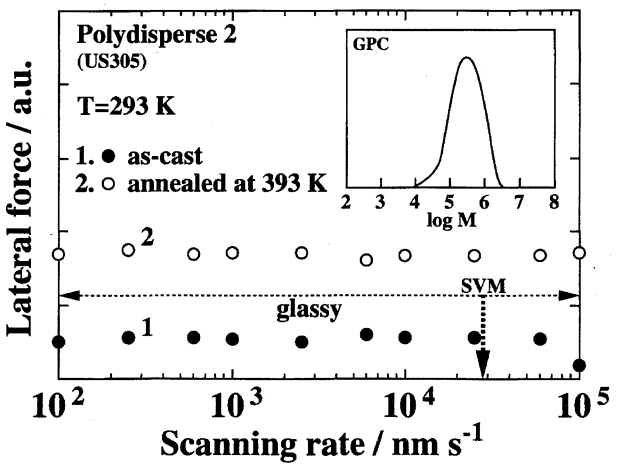


Fig. 17. Scanning rate dependence of lateral force for the Polydisperse 2 film at 293 K. The filled and the open circles denote the lateral force for the as-cast Polydisperse 2 film and annealed one at 393 K for 24 h, respectively. The inset in this Figure shows the molecular weight distribution of Polydisperse 2 system. The broken arrow in the Fig. 17 shows the scanning rate corresponding to the frequency of SVM measurement.

SVM measurements indicate that the surface of the Polydisperse 2 film is in a glassy state at 293 K. Then, it can be concluded that if the fraction of the lower molecular weight component than 30 k is very small, in spite of the broader molecular weight distinction, the surface molecular motion is not activated at room temperature due to the negligible surface localization of chain end groups.

**Surface Morphology and Surface Mechanical Properties of Polymer Blend Films.** The phase-separated surface structure for the polymer blend film has been studied on the basis of topographical and mechanical images obtained by AFM and SVM observations. The [polystyrene/poly(methyl vinyl ether)] [(PS/PMVE)] (62/38 w/w) blend film was prepared onto the hydrophilic substrate by a dip-coating method. Figure 18(a) shows the AFM image of the as-cast (PS/PMVE) (62/38) ultrathin film of 25 nm thick on the hydrophilic substrate. In this paper, the polymer blend films whose thicknesses are less than twice the radius of gyration of an unperturbed chain, 2Rg, of the longest component can be defined as two-dimensional blend films. AFM observation revealed that the (PS/PMVE) ultrathin film was in an apparent phase-separated state in which the droplet-like domains of 200—500 nm in diameter and 20—40 nm in height were formed. The mechanism of the ultrathining-induced surface phase separation for the (PS/PMVE) blend film was published elsewhere.[32] The characterization of the droplet-like domains was carried out using AFM observation of the (PS/PMVE) ultrathin film with different (PS/PMVE) blend ratios. The apparent surface area for the droplet-like domains on the AFM image decreased with a decrease in the PMVE weight fraction. Then, it is apparent from the AFM observation that the droplet-like domains composed of the PMVE rich phase.

SVM observations were performed in order to evaluate surface viscoelasticity of the as-cast (PS/PMVE) (62/38 w/w) ultrathin film of 25 nm thickness on the hydrophilic SiO substrate. Since the bulk $T_g$ of PS is far above room temperature, whereas that of PMVE is below room temperature, it is expected that the glassy PS and the rubbery PMVE phases can be distinguished apparently even at the surface, on the basis of the SVM observations. Figure 18(b) shows the two-dimensional image of a surface dynamic storage modulus $E'$ for the (PS/PMVE) ultrathin film at 293 K. The darker and the brighter regions correspond to the lower and the higher $E'$, respectively. The droplet-like domains in Fig. 18(b) correspond to those for the AFM image shown in Fig. 18(a). Therefore, it is reasonable to conclude from parts (a) and (b) of Fig. 18 as well as the variation of the domain-matrix area fraction that the droplet-like domains are composed of the rubbery PMVE rich phase and that the matrix is composed of the glassy PS one.

The contrast in AFM image means the difference of the sample height, whereas that in SVM image reflects the difference of $E'$. Then, the combination of AFM and SVM observations can tell us the interfacial characteristics of the two-phase system. For instance, SVM can show the surface phase separation based on the difference of $E'$, even in the

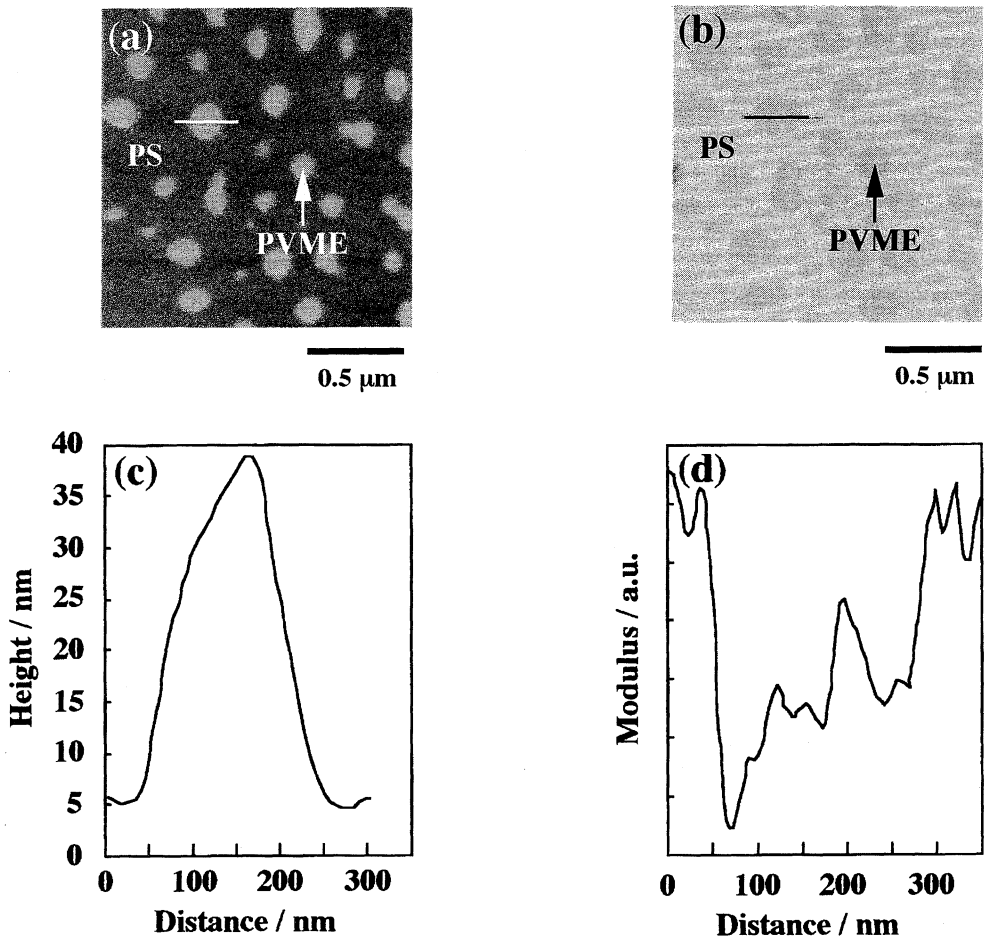


Fig. 18. (a) AFM topographic and (b) SVM $E'$ image for the (PS/PMVE) (62/38 w/w) ultrathin film. Parts (c) and (d) show the line profiles of height and modulus along the lines in the AFM and SVM images, respectively.

case that the height difference between domain and matrix is extremely small. Parts (c) and (d) of Fig. 18 show typical height and modulus profiles along the lines shown in Figs. 18(a) and 18(b), respectively. Figures 18(c) and 18(d) indicate that the radius of PMVE domain in the AFM image was smaller than that observed by SVM. Therefore, it is possible to discuss the interfacial structure at the phase-separated surface on the basis of the comparison between topographical and mechanical images. Figure 19 shows the schematic representation of the sectional profile of the two possible surface aggregation structure for the (PS/PMVE) blend ultrathin film. The model was drawn on the basis of the AFM and SVM observations, as mentioned above. The SVM results indicate either the presence of low modulus PMVE thin layer around the domain boundary, as shown in Fig. 19(a), or the compositional gradient structure along the radial direction of PMVE rich domain, as shown in Fig. 19(b). Further effort is in progress in order to distinguish these two models.

## Conclusion

LFM and SVM measurements for the monodisperse PS films, the binary and the ternary PS blend films and the polydisperse PS films were performed at 293 K in order to investigate the surface molecular motion. It was revealed that

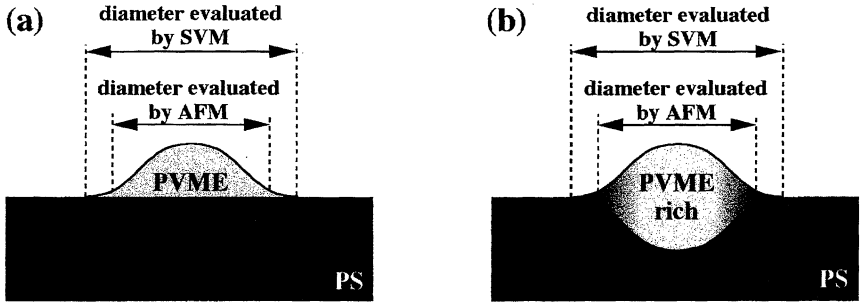


Fig. 19. Two-possible models of the cross-section for the phase-separated (PS/PMVE) ultrathin films.

the surface of the monodisperse PS film with $M_n$ less than ca. 30 k was in a glass–rubber transition state even at 293 K, due to an excess free volume at the air/polymer interface induced by the surface segregation of chain end groups. In the case of the binary and the ternary PS films, which are composed of PS with $M_n$ of 19.7 k and higher molecular weight PS, it was revealed that the surface was in a glass–rubber transition state at 293 K, due to the surface segregation of lower molecular weight component PS with $M_n$ of 19.7 k. In the case of the polydisperse PS film, although the surface molecular motion was activated in comparison with the bulk one, the surface dynamic viscoelastic variations that are characteristic of a glass–rubber transition state were not observed at 293 K in a similar fashion to that for the monodisperse PS film with $M_n$ less than ca. 30 k. The difference of the activation for the surface molecular motion between monodisperse and polydisperse PS films can be explained on the basis of the chemical structure of the chain end groups. Also, in the case of the broad molecular weight distribution, if there was not lower molecular weight component, the surface molecular motion was not apparently activated at room temperature.

Also, the combination of AFM and SVM observations can provide new and additional information on the interfacial structure of multiphase polymer which the individual AFM and SVM observation cannot detect, and can distinguish the phase-separated surface structure.

## References


1) W. J. Feast, H. S. Munro, and R. W. Richards, "Polymer Surface and Interfaces," Vol. 2, Wiley, New York (1993).

2) F. Grabassi, M. Morra, and E. Occhiello, "Polymer Surfaces," Wiley, New York (1994).

3) H. Nakanishi and P. Pincus, *J. Chem. Phys.*, **79**, 997 (1983).

4) R. A. L. Jones and E. J. Kramer, *Polymer*, **34**, 115 (1993).

5) K. Tanaka, A. Takahara, and T. Kajiyama, *Macromolecules*, **29**, 3232 (1996).

6) T. Kajiyama, K. Tanaka, S.-R. Ge, and A. Takahara, *Prog. Surf. Sci.*, **52**, 1 (1996).

7) T. Kajiyama, K. Tanaka, and A. Takahara, *Macromolecules*, **28**, 3482 (1995).

8) K. Tanaka, A. Takahara, and T. Kajiyama, *Acta Polym.*, **46**, 476 (1995).

9) G. Binnig, C. F. Quate, and C. G. Gerber, *Phys. Rev. Lett.*, **56**, 930 (1986).

10) H.-H Guntherodt and R. Weisendanger, "Scanning Tunneling Microscopy," Springer-Verlag, New York (1992—1993), Vols. I—III.

11) "STM and SFM in Biology," ed by O. Marti and M. Amrein, Academic Press, New York (1993).

12) P. Maivald, H. J. Butt, S. A. C. Gould, C. B. Prater, B. Drake, J. A. Gurley, V. B. Elings, and P. K. Hansma, *Nanotechnology*, **2**, 103 (1991).

13) M. Radmacher, R. W. Tillman, and E. Gaub, *Biophys. J.*, **64**, 735 (1993).

14) R. M. Overney, E. Meyer, J. Frommer, H.-J. Guntherodt, M. Fujihira, H. Takano, and Y. Gotoh, *Langmuir*, **10**, 1281 (1994).

15) T. Kajiyama, K. Tanaka. I. Ohki, S.-R. Ge, J.-S. Yoon, and A. Takahara, *Macromolecules*, **27**, 7932 (1994).

16) R. M. Overney, *Trends Polym. Sci.*, **3**, 359 (1995).

17) K. Tanaka, A. Taura, S.-R. Ge, A. Takahara, and T. Kajiyama, *Macromolecules*, **29**, 3040 (1996).

18) R. M. Overney, E. Meyer, J. Frommer, D. Brodbeck, L. Howald, H. Guntherodt, M. Fujihira, H. Takano, and Y. Gotoh, *Nature*, **359**, 133 (1992).

19) D. D. Koleske, W. R. Barger, and R. J. Colton,"AVS National Symp. Abstr., 42nd," NS+SS-TuA6 (1995).

20) K. A. Grosch, *Proc. R. Soc. London, Ser. A*, **274**, 21 (1963).

21) K. Minato and T. Takemura, *Jpn. J. Appl. Phys.*, **6**, 719 (1967).

22) G. Haugstad, W. L. Gladfelter, E. B. Weberg, R. T. Weberg, and R. R. Jones, *Langmuir*, **11**, 3473 (1995).

23) R. Wiesendanger, "Scanning Probe Microscopy and Spectroscopy Methods and Applications," Cambridge University Press, New York (1994).

24) K. Tanaka, A. Takahara, and T. Kajiyama, *Kobunshi Ronbunshu*, **53**, 582 (1996).

25) H. Hertz, *J. Reine Angew. Math.*, **92**, 156 (1882).

26) S. Naganuma, T. Sakurai, Y. Takahashi, and S. Takahashi, *Kobunshi Kagaku*, **29**, 105 (1972).

27) I. M. Ward and D. W. Hadley, "An Introduction to the Mechanical Properties of Solid Polymers," John Wiley & Sons, Chichester, U. K. (1993).

28) In order to investigate the scanning rate dependence of adhesion force, LFM measurement of the silicon wafer, which did not show viscoelastic properties and any scanning rate dependence of lateral force, was carried out under same condition as measurement of the monodisperse PS film. Since the scanning rate dependence of lateral force was not observed, it seemed reasonable to conclude that the scanning rate dependence of adhesion force was negligible in this scanning rate regio.

29) K. Tanaka, A. Takahara, and T. Kajiyama, in preparation.

30) P.-G. de Gennes, "Physics of Pomer Surfaces and Interfaces," Butterworth-Heinemann, Boston (1992).

31) S. Wu, "Polymer Interface and Adhesion," Marcel Dekker, New York (1982).

32) K. Tanaka, J.-S. Yoon, A. Takahara, and T. Kajiyama, *Macromolecules*, **28**, 934 (1995).

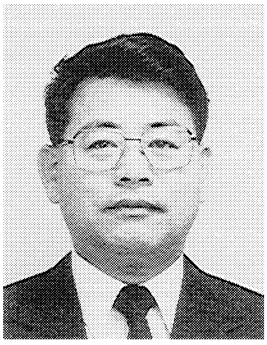

Tisato Kajiyama, Professor, Department of Materials Physics and Chemistry, Kyushu University, received Ph.D. degrees from the University of Massachusetts in 1969 (Polymer Physics) and from Kyushu University in 1975 (Polymer Chemistry). Major research areas are 1) viscoelastic properties of crystalline polymers, 2) molecular aggregation state-mechanical property relationships of molecular composites, 3) fatigue analysis of solid polymers, 4) surface characterization of polymers, 5) structure-property relationships of monolayer and LB films, and 6) functional properties of polymer/(liquid crystal) composite systems.

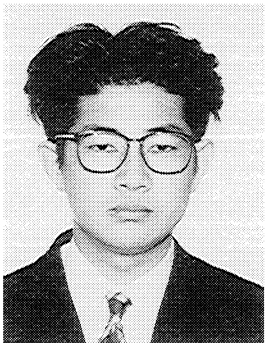

Keiji Tanaka, Fellow of the Japan Society for the Promotion of the Science, Department of Materials Physics and Chemistry, Kyushu University, received a Ph.D. degree from Kyushu University in 1997 (Polymer Chemistry). His major research area is the surface characterization of polymers.

Atsushi Takahara, Associate Professor, Department of Materials Physics and Chemistry, Kyushu University, received a Ph.D. degree from Kyushu University in 1983 (Polymer Chemistry). Major research areas are the non-linear viscoelasticity of solid polymers, the surface characterization of polymers, and the characterization of organic ultrathin films.